High-resolution EPMA X-ray images of mother liquid inclusions in a Pd_2Ga single crystal

2014 IOP Conf. Ser.: Mater. Sci. Eng. 55 012013

(http://iopscience.iop.org/1757-899X/55/1/012013)

High-resolution EPMA X-ray images of mother liquid inclusions in a Pd_2Ga single crystal

D Müller[1], J Schwerin[2], P Gille[2] and K T Fehr[1]

[1] Ludwig-Maximilians-Universität, Department of Earth and Environmental Sciences, Section for Mineralogy, Theresienstrasse 41, DE-80333 Munich, Germany
[2] Ludwig-Maximilians-Universität, Department of Earth and Environmental Sciences, Crystallography Section, Theresienstrasse 41, DE-80333 Munich, Germany

E-mail: dirk.mueller@min.uni-muenchen.de

Abstract. During crystal growth from solution inclusions of different compositions were trapped at the rim of a Pd_2Ga single crystal. Their fine-grained (< 5 µm) internal structure demands special requirements for electron microprobe analysis, realized by low-voltage (5 keV) element mapping applying a step size of 0.138 µm for each pixel. It can be shown, that these inclusions represent an isolated chemical system, and that crystallisation upon cooling follows the expected thermodynamic phase relations. Thus the final composition in the centre of the inclusion consists of a small-scale mixture of PdGa and Pd_5Ga_3 evolved out of a solid-solid decomposition of Pd_5Ga_4.

1. Introduction

Pd_2Ga has a high potential to be utilized as a next generation catalytic material in the production process of polyethylene, where pure Pd or alloyed catalysts are presently in use [1]. In view of a polyethylene production of 50 megatons per year, it is quite a huge business in the chemical industry [2]. This makes it necessary to improve catalysts to increase the output, reduce production cost and save the environment [3].

The semi-hydrogenation of acetylene is a necessary step in removing minor amounts of acetylene from the ethylene feed during the production of polyethylene. It is important to decrease the acetylene content from 1 % to a very low ppm range; otherwise it would deactivate the catalyst [1, 2]. Today, commercial catalysts show a high hydrogenation-activity but a limited selectivity to ethylene. In recent years the intermetallic compound Pd_2Ga (space group Pnma, Co_2Si structure type [4]) has been explored as a highly selective heterogeneous hydrogenation catalyst. Compared to currently used catalysts, the intermetallic compound shows an improved long-term stability as well as a high selectivity and activity. These outstanding properties can be explained by covalent bonding interactions and the well-defined crystal structure with fixed sites of the catalytically active element Pd [1-3, 5], also known as active-site isolation concept [6].

Due to higher specific area these intermetallic compounds will finally be used as fine-grained powders or even nanoparticles. To determine their intrinsic properties and basic processes of catalysis, however, it is necessary to investigate well-defined single crystals of cm^3-size. In order to grow such large single crystals the Czochralski method was used.

According to the phase diagram (figure 1), the orthorhombic solid-solution (ss) phase Pd_2Ga can be grown from a congruent melt or from Ga- or Pd-rich high-temperature solutions. Due to the Ga

vapour pressure, crystallisation from Ga-rich solution at lower temperatures is preferable. During post-growth cooling this could lead to precipitations of the orthorhombic solid-solution phase Pd_5Ga_3 (space group Pbam, Ge_3Rh_5 structure type [7]), which makes it is necessary to check the crystal composition by electron probe microanalysis (EPMA).

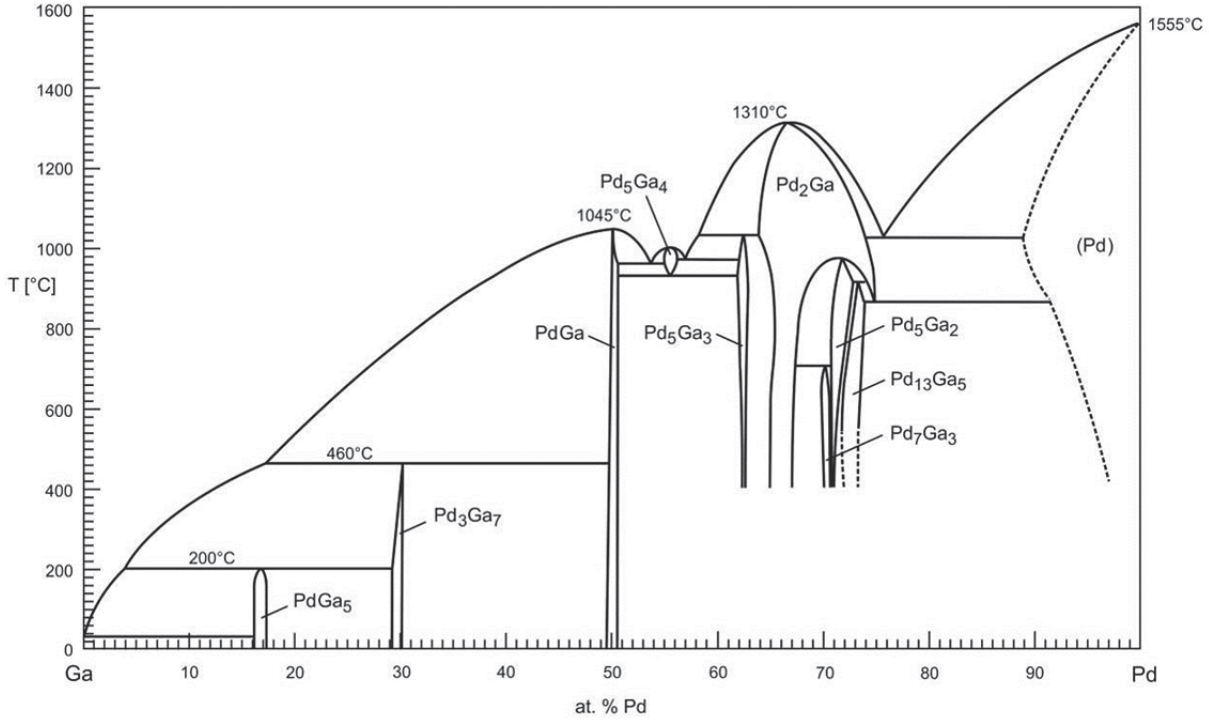

Figure 1. Phase diagram of Ga-Pd [9]

The challenge for EPMA investigations of these inclusions is their fine-grained mixture of different phases. To increase X-ray resolution, beam voltage has to be reduced as low as possible and practicable. Applying a low overvoltage ratio would further improve the spatial resolution of the analysis [8]. Using a LaB_6 electron source the measurement presented here was restricted to the low beam voltage method at commonly used overvoltage ratios of 1.6 - 4.5. In this paper a fully quantitative, high-resolution element mapping was carried out, working at the limits of a LaB_6-equipped electron microprobe.

2. Experimental

2.1. Crystal growth

The Czochralski method is one of the most famous and best studied methods for the production of large single crystals of different compositions. The working principle is shown in figure 2: a well oriented seed (a) is dipped in the molten source material (c). Due to marginal undercooling crystallisation starts on the thin neck of the seed. Subsequently the seed, together with the attached grown crystal (b), is slowly pulled upward while the crystal is growing. For a homogeneous mixture of the source material it is crucial to rotate the crystal in counter direction to the crucible during the whole experiment. The diameter was controlled by adjusting the temperature, while the pulling rate was fixed to 0.15 mm/h. The initial composition of the solution was $Pd_{61.4}Ga_{38.6}$.

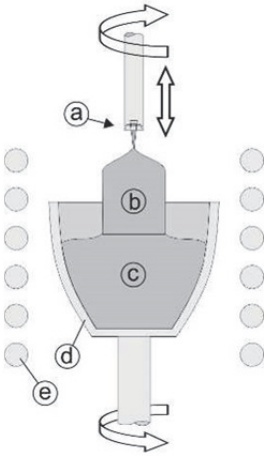

Figure 2. Working principle of the Czochralski method. The arrows on top and bottom symbolize the counter rotation of crystal and crucible. a) seed, fixed in a seed holder; b) grown crystal; c) molten source material; d) inert crucible; e) heating elements.

2.2. Analytical procedure

For EPMA analysis a thin slice was cut from the end of the single crystal (figure 3) and polished using diamond paste of decreasing grain size down to 0.25 µm to obtain a flat surface. Carbon coating was unnecessary as the sample is naturally conductive. The measurements were carried out on a Cameca SX-100 system, equipped with a LaB_6 cathode. An accelerating voltage (E_0) of 5 keV at a current of 20 nA was used. These values were chosen based on the critical excitation voltage (E_c) of the respective elements: Pd Lα - 3.173 keV and Ga Lα - 1.117 keV. To excite X-rays of an adequate amount a sufficient ionisation cross-section has to be reached, depending on the applied overvoltage ratio. This could be calculated from eq. (1), where U is the overvoltage ratio (E_0/E_c) [10]. At 5 keV $U_{PdL\alpha} = 1.58$ and $U_{GaL\alpha} = 4.48$ which gives practicable ionisation cross-sections for both elements of $QE_c^2{}_{PdL\alpha} = 2.30$ (10^{-20} cm^{2}keV^2) and $QE_c^2{}_{GaL\alpha} = 2.65$ (10^{-20} cm^{2}keV^1), respectively.

$$QEc^2 = 7.92 \cdot 10^{-14} \ln U \cdot U^{-1} \quad (1)$$

Figure 3. Pd_2Ga solid-solution single crystal grown by the Czochralski method from Ga-rich solution. The marked section represents the investigated slice of the crystal.

Due to the small grain size and heterogeneous distribution of the two phases a quantitative element mapping is preferable in contrast to single point measurements. Therefore, Pd and Ga were analysed simultaneously on two different wavelength-dispersive X-ray spectrometers (WDS). The Pd Lα-line was measured on a LPET and the Ga Lα-line on a TAP crystal. The mapping represents an area of 30 µm x 30 µm, analysed by a grid of 230x230 pixels with a dwell time of 0.07 s for each pixel. This gives a spatial resolution (pixel width) of 0.131 µm, which is in the range of the theoretical resolution for the expected composition of the sample (Table 1), calculated from eqs. (2) - (4). For comparison it should be noted that only eq. (4) accommodates the beam diameter:

Reed 1975 [10] $$d = 0.231\ (E_0^{1.5} - E_c^{1.5}) \cdot \rho^{-1} \quad (2)$$

Gauvin 2007 [11] $$d = k\ (E_0^{n} - E_c^{n}) \cdot \rho^{-1} \quad (3)$$

Merlet & Llovet 2012 [12] $$d = \sqrt{4\ (33\ A\ (E_0^{1.7}\text{-}E_c^{1.7}) \cdot (\rho\ Z)^{-1}\text{-}Z_m)^2 + d_0^2} \quad (4)$$

in which ρ denotes for the density of the investigated phase (ρ_{PdGa} = 9.97 g·cm^{-3}; ρ_{Pd5Ga3} = 10.73 g·cm^{-3}). These values are X-ray densities, calculated on the basis of structure models. *k* and *n* in eq. (3) are variables that were calculated using the equations given in [11]. In eq. (4), *A* is the atomic weight [g·mol^{-1}], *Z* the atomic number, and d_0 the beam diameter, that was assumed to be 100 nm. *Zm* is the depth at which the X-ray distribution curve exhibits its maximum. Mapping was done using the beam scanning method (fixed stage, moving beam). The background was measured on the right side (lower energy) of the peak, applying the same dwell time per pixel of 0.07 s as suggested by [13]. The conversion of raw counts to element concentrations was processed with the PAP matrix correction [14]. The influence of fluorescence would have only a minor impact on the analysis results and was, therefore, not investigated in detail. Calibration was done on pure Pd and stoichiometric PdGa. A peak overlap correction was not necessary.

Table 1. Calculated spatial X-ray resolution d (µm) for Pd and Ga in PdGa and Pd_5Ga_3, derived from different calculation procedures.

	Reed 1975		Gauvin 2007*		Merlet & Llovet 2012	
	d_{PdGa}	d_{Pd5Ga3}	d_{PdGa}	d_{Pd5Ga3}	d_{PdGa}	d_{Pd5Ga3}
Pd	0.128	0.119	0.065	0.061	0.162	0.155
Ga	0.232	0.215	0.105	0.097	0.234	0.221

* to compare these values with results from eqs. (2) and (4) a beam diameter of 100 nm has to be added

2.3. Image processing

Applying low voltage, current and counting times the peak to background ratio and the precision is decreasing, leading to noisy images. A powerful mathematical approach to improve the image quality is the Kriging analysis [15], which was used for the post-measurement processing of the results presented here. First developed for the classification of ore bodies [16] this method became a widespread application for analysing spatially distributed data.

The computed variogram, representing the variance of pairs of variates in relation to their spatial distribution, was modelled applying the nugget effect to remove the noise and a Cauchy function to reduce measurement artefacts. To smooth the image, a neighbourhood filter was used.

3. Results

Inclusions are observed at the rim of the $(Pd_2Ga)_{ss}$ single crystal (figure 4). The maximum diameter of individual inclusions is approximately 300 µm. Most of them show a circular shape and an internal separation, consisting of a homogeneous outer part and a heterogeneous core, comprising a porphyric structure of larger crystals of $(Pd_5Ga_3)_{ss}$ in a fine grained mixture of $(Pd_5Ga_3)_{ss}$ and $(PdGa)_{ss}$, respectively (figures 4 and 5). The homogenous outer region consists of several areas with different backscattered electron (BSE) intensities (different grey levels) suggesting a heterogeneous composition. Quantitative EPMA point analyses, however, indicate that these areas have the same composition, according to $(Pd_5Ga_3)_{ss}$. Thus, this effect could be explained by different crystal orientations (channelling effect) [17].

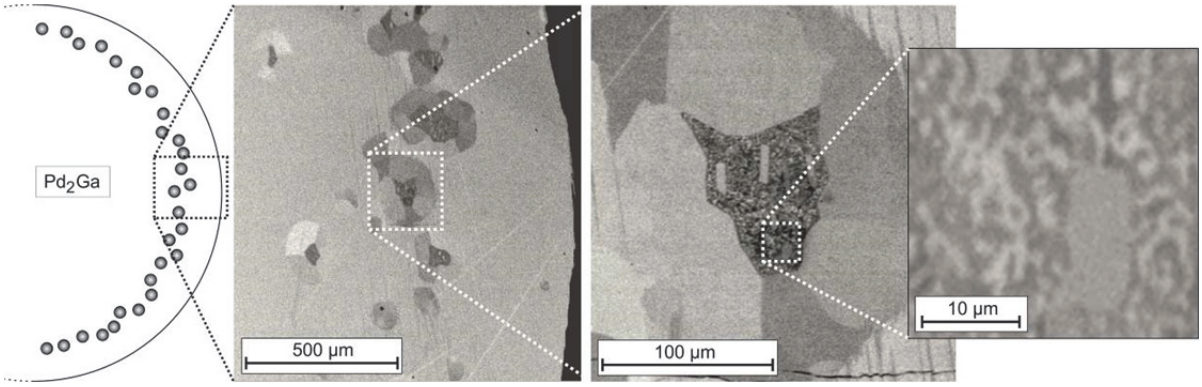

Figure 4. Appearance of Ga-enriched mother liquid inclusions in the $(Pd_2Ga)_{ss}$ single crystal. Their internal structure consists of an outer shell of $(Pd_5Ga_3)_{ss}$ containing a core of $(Pd_5Ga_3)_{ss}$ and $(PdGa)_{ss}$ (visible in the BSE images). The zoomed box on the right shows the mapped area.

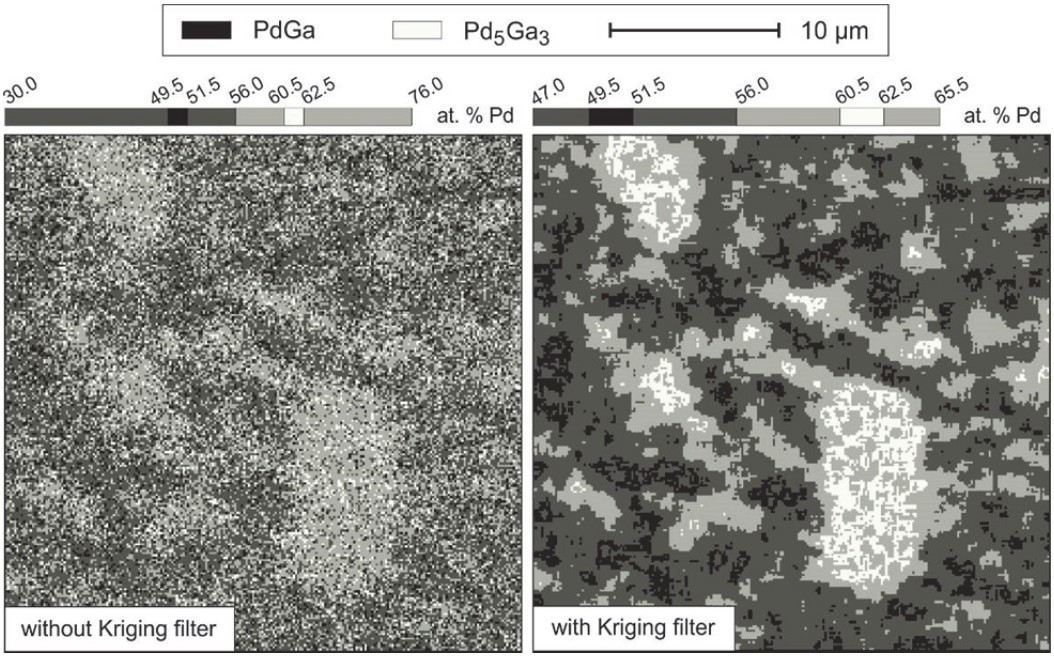

Figure 5. Quantitative X-ray images of the fine grained mixture of $(Pd_5Ga_3)_{ss}$ and $(PdGa)_{ss}$ in the core of the inclusion. Left: without Kriging analysis, showing a noisy, pixelated image. Right: image after Kriging analysis applying a 5x5 neighbourhood filter. Dark grey and light grey colours represent the systematic error of the measurement.

The element mapping was conducted in the core of an inclusion, covering an area which comprises bigger Pd_5Ga_3 crystals as well as the fine grained matrix of $(Pd_5Ga_3)_{ss}$ and $(PdGa)_{ss}$. The brighter regions and crystals in figure 4 represent the Pd-rich phase $(Pd_5Ga_3)_{ss}$ and the darker sections are $(PdGa)_{ss}$. The larger crystals reach a size up to 35 µm in length and 9 µm width, whereas in other inclusions they could be even larger (up to 90 µm). The irregular pattern of the two phases shows different grain sizes below 5 µm.

Figure 5 shows the lateral phase distribution which is in good agreement with the BSE image of figure 4. Regarding the phase diagram in figure 1 the composition of $(PdGa)_{ss}$ is 50.5 at% Pd and for $(Pd_5Ga_3)_{ss}$ 61.5 at% Pd. Taking a random error of ±1 at% into account, these values widen up to 49.5 - 51.5 at% Pd for PdGa and 60.5 - 62.5 at% Pd for Pd_5Ga_3, respectively. Without Kriging analysis a large systematic error is observable resulting in a wide compositional range from 30.0 - 76.0 at% Pd. After applying the Kriging filter the range of composition is limited to 47.0 - 65.5 at% Pd giving a more precise image. The choice of a suitable neighbourhood filter was done empirically by evaluating the area covered from the two phases (figure 6). Since this ratio is no longer changing at values higher than a 5x5 matrix, this filter was chosen as an optimum for the image in figure 5.

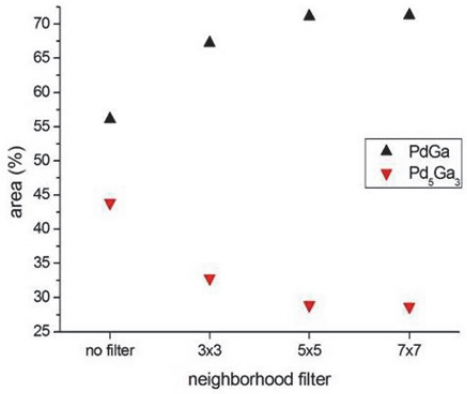

Figure 6. Impact of Kriging analysis on area coverage of $(PdGa)_{ss}$ and $(Pd_5Ga_3)_{ss}$. Neighbourhood filters regarding a matrix of > 5x5 pixels show no significant change anymore.

4. Discussion

The varying sizes of different inclusions and also the presence or absence of bigger $(Pd_5Ga_3)_{ss}$ crystals in the core could be explained by the cutting effect. Presuming a truly spherical shape, the complete content is only visible if the inclusion was cut through the centre (representing the full radius), which depends on their statistical distribution within the single crystal.

The best agreement between BSE and X-ray image could be observed in the central region of the mapped area (figure 5). By applying the Kriging filter the separation of the two phases reveals details more clearly. Based on this EPMA mapping, the internal evolution of these inclusions could be derived. After having been trapped, the liquid inclusion (1) follows the complete crystallisation path, visible in the phase diagram of figure 7: the inclusion represents a closed chemical system. While cooling down (1→2) $(Pd_2Ga)_{ss}$ will form until the temperature reaches the peritectic point (2). Due to the same composition and probably homo-epitaxial growth, this first rim could not be detected with EPMA. At the peritectic temperature $(Pd_5Ga_3)_{ss}$ crystallizes according to the peritectic reaction and simultaneously separates the liquid from the first grown $(Pd_2Ga)_{ss}$ crystal and preserves it from partial dissolution. An on-going cooling along with the crystallisation of $(Pd_5Ga_3)_{ss}$ brings the system to the eutectic point (3), which leads to an abrupt consumption of the remaining melt by the formation of $(Pd_5Ga_3)_{ss}$ and $(Pd_5Ga_4)_{ss}$ crystals. Obeying the lever rule more $(Pd_5Ga_4)_{ss}$ and less $(Pd_5Ga_3)_{ss}$ will be formed. Reaching the eutectoid point at (4) the $(Pd_5Ga_4)_{ss}$ phase decomposes into $(Pd_5Ga_3)_{ss}$ and $(PdGa)_{ss}$ at subsolidus conditions. Due to the relatively low temperatures the diffusivity of the elements during this solid-solid reaction is quite low and leads to the small-scale dissolution structures discussed above.

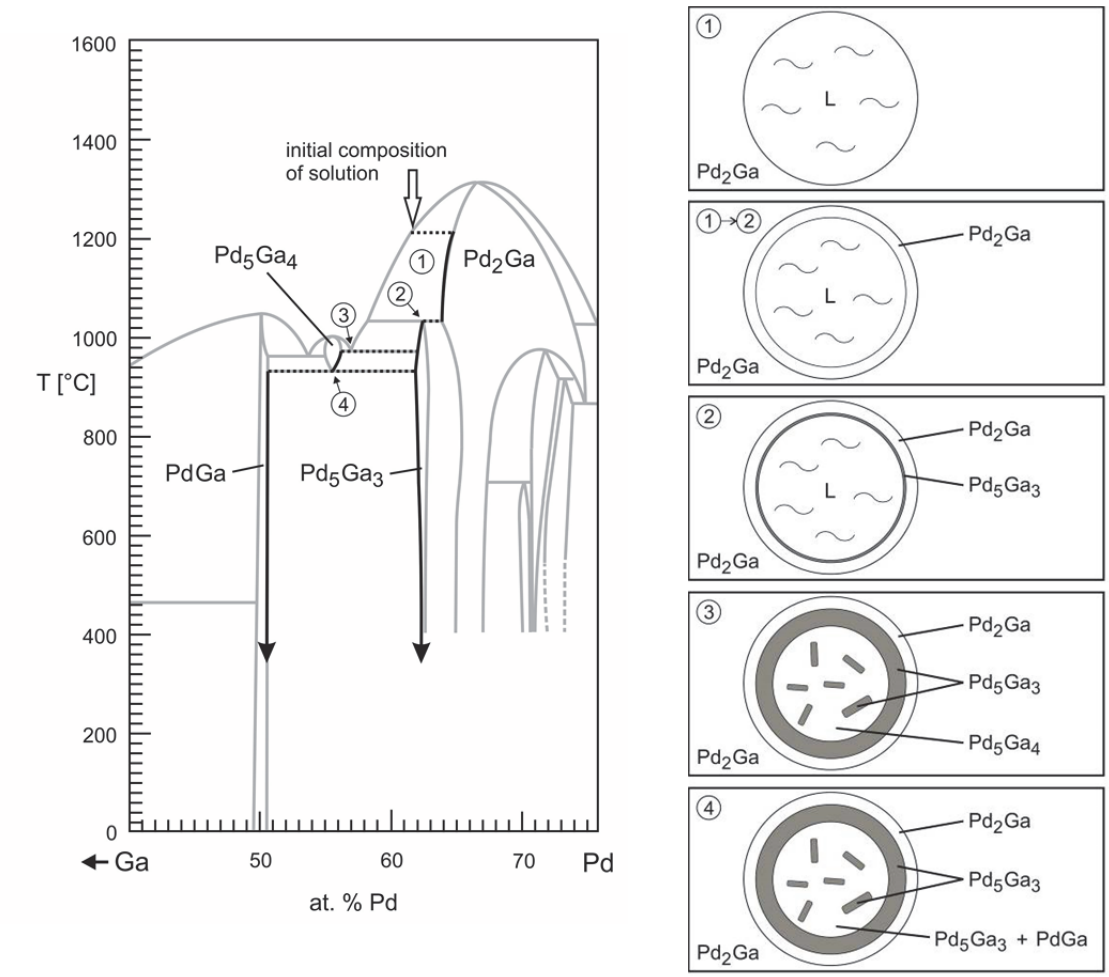

Figure 7. Section of the Ga-Pd phase diagram in the range of 40- 76 at% Pd. Continuous black lines show the crystallisation path of the inclusions during crystal growth while cooling down. Dotted lines represent separation processes. The single steps (1→4) of internal evolution of one single inclusion is shown on the right. L – liquid.

Inclusion formation is a quite common defect in solution growth and can be explained by an insufficient mixing of the solution during the growth process, namely of the rejected solvent adjacent to the growth interface. The rotation of crystal and crucible together with a curved solid-liquid interface leads to the circular arrangement at the rim of the crystal. To avoid this process, the pulling rate has to be lowered, which was successfully done in subsequent experiments.

5. Conclusion

A complete chemical characterisation of the inclusions was possible. On the basis of these results the entire development of the inclusions could be deduced which is in good agreement with the phase diagram. As a consequence, the crystal growth parameters could be optimized to avoid such inclusions in future.

Further improvement of the X-ray resolution might be achieved by reducing the accelerating voltage and the current, which implies longer analysis time and the use of a field-emission (FE) electron-gun. Due to a two-component system it would be possible to measure the Ga-content only

and conclude the total composition of the specimen from these values. This would give the possibility to further decrease the accelerating voltage.

Acknowledgement
The authors would like to thank Michael Hahne and Birgitta Meisterernst for helpful discussions and suggestions regarding crystallographic topics. Helpful comments of Xavier Llovet and two anonymous reviewers to improve the paper are gratefully acknowledged. Thanks also to Renate Enders for her assistance in the preparation of the samples.

This work has been partly conducted within the European integrated Centre for the development of new Metallic Alloys and Compounds (European C-MAC).

References

[1] Armbrüster M, Wowsnick G, Friedrich M, Heggen M and Cardoso-Gil R 2011 *J. Am. Chem. Soc.* **133** 9112
[2] Armbrüster M, *et al.* 2012 *Chem. Cat. Chem.* **4** 1048
[3] Kovnir K, Osswald J, Armbrüster M, Teschner D, Weinberg G, Wild U, Knop-Gericke A, Ressler T, Grin Yu and Schlögl R 2009 *J. Catal.* **264** 93
[4] Kovnir K, Schmidt M, Waurisch C, Armbrüster M, Prots Yu and Grin Yu 2008 *Z. Kristallogr.-New Cryst. Struct.* **223** 7
[5] Osswald J, Giedigkeit R, Jentoft R E, Armbrüster M, Girgsdies F, Kovnir K, Ressler T, Grin Yu and Schlögl R 2008 *J. Catal.* **258** 210
[6] Sachtler W M H 1976 *Catal. Rev. Sci. Engng.* **14** 193
[7] Schubert K, Breimer H, Gohle R, Lukas H L, Meissner G and Stolz E 1958 *Naturwissensch.* **45** 360
[8] Newburry D E 2002 *Microsc. Microanal.* **8**, Suppl. 2, 434
[9] Okamoto H 2008 *J. Phase Equilib. Diffus.* **29** 466
[10] Reed S J B 1975 *Electron microprobe analysis*. (Cambridge: Cambridge University Press) 198
[11] Gauvin R 2007 *Microsc. Microanal.* **13** 354
[12] Merlet C and Llovet X 2012 *IOP Conf. Series: Mat. Sci. Engng.* **32** 012016
[13] Reed S J B 2000 *Mikrochim. Acta* **132** 145
[14] Pouchou J L and Pichoir F 1984 *Rech. Aérosp*. **3** 167
[15] Mainy D, Nectoux J P and Renard D 1996 *Mater. Charact.* **36** 327
[16] Matheron G 1965 *Les variables régionalisées et leur estimation*. (Paris: Masson) 306
[17] Meisenkothen F, Wheeler R, Uchic M D, Kerns R D and Scheltens F J 2009 *Microsc. Microanal.* **15** 83